

Fractional instanton of the SU(3) gauge theory in weak coupling regime

Etsuko Itou ♣,♥,♠

♣ Department of Physics, and Research and Education Center for Natural Sciences, Keio University, 4-1-1 Hiyoshi, Yokohama, Kanagawa 223-8521, Japan

♥ Department of Mathematics and Physics, Kochi University, Kochi 780-8520, Japan

♠ Research Center for Nuclear Physics (RCNP), Osaka University, Osaka 567-0047, Japan

E-mail: itou@yukawa.kyoto-u.ac.jp

November 15, 2018

Abstract

Motivated by recent studies on the resurgence structure of quantum field theories, we numerically study the nonperturbative phenomena of the SU(3) gauge theory in a weak coupling regime. We found that topological objects with a fractional charge emerge, if the theory is regulated by an infrared (IR) cutoff via the twisted boundary condition. Some integer-instantons are generated as a semi-classical configuration in the Montecarlo simulation even in the weak coupling regime. Furthermore, some of them consist with several fractional-instantons. We also measure the Polyakov loop to investigate the center symmetry and confinement. The fractional-instanton corresponds to the solution linking two of degenerate \mathbb{Z}_3 -broken vacua in the deconfined phase.

1 Introduction

Instanton is one of the classical solutions of the quantum field theory, and labels a vacuum state. In pure Yang-Mills theory in the four-dimensional Euclidean spacetime (\mathbb{R}^4), the instanton has a topological charge (instanton number) given by

$$Q = \frac{1}{32\pi^2} \int d^4x \epsilon_{\mu\nu\rho\sigma} F_{\mu\nu}^a F_{\rho\sigma}^a, \quad (1)$$

where $\epsilon_{\mu\nu\rho\sigma}$ denotes a totally anti-symmetric tensor. It always takes an integer value [1]. In fact, the topological charge has been measured by the lattice *ab initio* calculations [2]. The distribution of Q is broad in the hadronic (confined) phase in the low temperature, while it is narrow in the quark-gluon-plasma (deconfined) phase in the high temperature [3, 4]. According to the lattice numerical study [5, 6], it is also known that the first-order phase transition occurs between these phases in the pure SU(3) gauge theory.

Actually, most lattice calculations have been performed on the hypertorus (\mathbb{T}^4) with the standard periodic boundary condition, though the Yang-Mills theory on the periodic hypertorus does not have a self-dual configuration as a classical solution. To obtain a stable $Q \neq 0$ configuration on the finite lattice, we have to impose the *twisted* boundary conditions [7]. The reason, why the ordinary lattice calculation with the periodic boundary condition can observe the nontrivial- Q solutions and the distribution of Q , is that the boundary effect is negligible in the strong coupling regime, where we have mainly focused on in the nonperturbative studies of the Yang-Mills theory.

The question arises as to the property of the topological objects in the weak coupling regime of the Yang-Mills theory. To see the quantities in the perturbative regime on the lattice, for instance to calculate of the running coupling constant, we need to set the renormalization scale to be higher than the Lambda scale (Λ). The renormalization scale is inversely proportional to the spacial lattice extent (L_s), so that we have to use the lattice extent satisfying $L_s \ll 1/\Lambda$. We expect that the choice of the boundary condition in such a small box must have an influence on the property of classical solution. Then, we have to consider which is a proper boundary condition to investigate the weak coupling regime. In fact, to realize the matching with the perturbative calculation on \mathbb{R}^4 , we need to utilize the nontrivial boundary conditions on hypertorus. Otherwise, the classical solution does not connect to the standard perturbative vacuum [7, 8, 9] because of a gauge

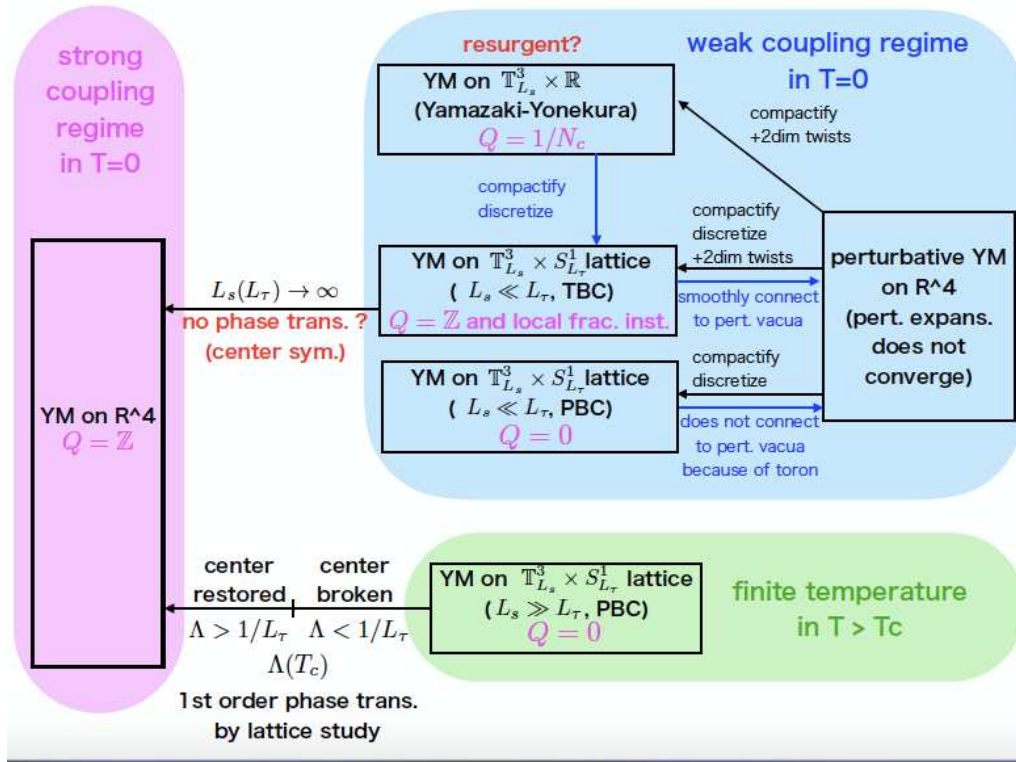


Figure 1: A roadmap to see a resurgence structure for the Yang-Mills theory. In this work, we focus on two boxes in the center.

inequivalent configuration, which is called *toron*, of the degenerate minimal action [10, 11]. For instance, the Schrödinger functional boundary [12, 13] or the twisted boundary conditions [14, 15] have been introduced in the calculation of the running coupling constant.

On the other hand, it is well-known that the perturbative expansion of the $SU(N_c)$ gauge theory on \mathbb{R}^4 spacetime does not converge in the higher order approximation. To solve this, for the quantum mechanical models and low-dimensional quantum field theories, which suffer from a similar problem, the resurgence scenario has been proposed [16, 17]. In the scenario, as a proper choice of the spacetime structure, a *compact dimension and/or a boundary condition with \mathbb{Z}_N -holonomy* are introduced. Then, the perturbative series and the nonperturbative effects of the theory on the modified spacetime are related to each other in the weak coupling regime, and the physical quanti-

ties are determined without any imaginary ambiguities. The characteristic phenomenon in the nonperturbative side of this scenario is the appearance of the topological objects with a local *fractional* charge, which contribute to the perturbative vacua, in (semi)-classical solutions of the theory. The fractionality of the topological charge is related to the cancelation of the renormalon pole [18, 19] whose action is of order $1/N_c$ in comparison with the action for the integer-instantons [20]. Recently, the resurgence structure has been revealed in several quantum-mechanical models and low-dimensional quantum field theories [20, 21, 22, 23, 24, 25, 26, 27, 28, 29]. Using the lattice numerical simulation, a signal of the fractional behavior for the energy density has observed in the Principle Chiral Model [30].

For the gauge theory, a recent paper [31] has proposed a promising regularization formula on $\mathbb{T}^3 \times \mathbb{R}$. The authors pointed out that the IR cutoff is necessary, which should be a higher energy scale than the dynamical IR scale, namely Λ scale, otherwise the trans-series expansion of physical observables breaks down in the Yang-Mills theory. Therefore, they introduce the twisted boundary conditions for the two compactified dimensions using one-form center symmetry. The twisted boundary condition induces the IR cutoff to the theory, and in the nonperturbative side the fractional instanton is allowed in the weak coupling regime. Furthermore, the center symmetry is dynamically restored because of the tunneling behavior between Z_{N_c} -degenerated vacua. It seems to be a promising to discuss the adiabatic continuity, where no phase transition occurs toward the decompactified limit in contrast with the first order phase transition at the finite-temperature. Although the resurgence structure of the Yang-Mills theory on the modified spacetime has not yet been proven, these phenomena are very similar with the ones in low-dimensional models, which are successfully resurgent.

According these situations, in this work, we formulate of the lattice gauge theory on $\mathbb{T}^3 \times S^1$ and study its nonperturbative properties by the numerical simulation. We summarize the relationship among several theories and lattice setups, that we mention above, in Fig. 1. This work corresponds to the second box in the center column in Fig. 1. Here, we maintain a large aspect ratio between two radius for the three-dimensional torus (L_s) and the temporal circle (L_τ) as $L_s \ll L_\tau$. We utilize the same twisted boundary condition as the one in Ref. [31]. Actually, we have already studied the running coupling constant of the Yang-Mills theory by using the same boundary condition in Ref. [15], so that we can tune the lattice parameter to be a weak coupling regime. The spacetime structure will be equivalent with the one in Ref. [31]

in the continuum and $S^1 \rightarrow \mathbb{R}$ limits. As a comparison, we also perform the ordinary periodic-lattice simulation with the same lattice parameter (third box in the center column in Fig. 1) and show the different nonperturbative-phenomena from the ones on the twisted lattice. The search for the fractional topology and the research of the basic properties of the Yang-Mills theory on the twisted lattice are interesting in itself. Furthermore, it is a challenge to define a regularized Yang-Mills theory from the perturbative to the non-perturbative regimes, although two parts with the question-mark in Fig. 1, namely the resurgent structure of the modified theory proposed in Ref. [31] and its adiabatic continuity, remain to be proven.

To show whether the configurations with fractional charge are generated, we directly measure the topological charge of configurations on the twisted lattice. We find that the multi-fractional-instanton solutions exist in the nontrivial- Q configurations even in the weak coupling regime. The total topological charge Q takes an integer-value as in the strong coupling regime in the ordinary periodic lattice, but some of them consist of several fractional-instantons. Furthermore, we also study the relationship between the fractional-instantons and the other nonperturbative phenomena, namely the tunneling behavior, the center symmetry, and the confinement. The fractional-instanton connects two of the degenerated \mathbb{Z}_{N_c} -broken vacua. By investigating the scaling law of Polyakov loop, we conclude that although the center symmetry seems to be partially restored, the free-energy of single probe quark is still finite and it is consistent with the deconfinement behavior.

The structure of the paper is as follows: In §. 2, we give a review of the twisted boundary conditions for the two compactified directions on the lattice. The toron configurations get a higher energy than the perturbative one and the gluon propagator does not have the zero-mode in the lattice setup. We give a comment on the absence of the zero-mode, which is related with the existence of the fractional-instanton as shown in Ref. [31]. In §. 3, the strategy of the Montecarlo simulation is explained. We tune the simulation parameters to be in the perturbative regime ($g^2 \approx 0.7$) in the large extent enough to generate multi-instanton configurations. We also describe our sampling method for a tiny lattice spacing with a long autocorrelation. Section 4 presents the simulation results. In §. 4.1, the nontrivial- Q configurations show up on the twisted lattice in the weak coupling regime, while there is no such configuration on the ordinary periodic lattice with the same lattice parameters. We find the local topological object with a fractional charge in the nontrivial solutions. The Polyakov loop distribution on the

twisted lattice has the different behavior from the periodic case as shown in §. 4.2. We describe the tunneling structure between the \mathbb{Z}_{N_c} -degenerated vacua by studying the local topological charge and the Polyakov loop on each site in §. 4.3. In §. 4.4, the deconfinement property of these configurations is discussed. The last section contains the summary and several future directions.

2 Twisted boundary condition on hypertorus lattice

We review the properties of the lattice gauge theory with the two-dimensional twisted boundary condition. On the hypertorus with the ordinary periodic boundary condition, the saddle points, which we would like to study their fluctuations in the perturbation expansion, are not only degenerated through gauge transformations, but an extra degeneracy exists due to the global toroidal structure [10, 11]. The configuration related with a part of the zero-mode is called toron. The toron configuration, however, has the higher energy than the vacuum one by the two-dimensional twisted boundary condition. Simultaneously, the gluon propagator is regulated by an IR momentum cutoff [9, 14, 15]. We also review the typical property of the fractional instanton related with the IR momentum cutoff given in Ref. [31].

Let us start the Wilson-Plaquette lattice gauge action for the Yang-Mills gauge theory;

$$S_W = \frac{2N_c}{g_0^2} \sum_{n, \mu > \nu} \left(1 - \frac{1}{N_c} \text{Tr} P_{\mu\nu}(n) \right). \quad (2)$$

Here, g_0 and $P_{\mu\nu}$ denote the lattice bare coupling constant and the plaquette,

$$P_{\mu\nu}(n) = U_\mu(n)U_\nu(n + \hat{\mu})U_\mu^\dagger(n + \hat{\nu})U_\nu^\dagger(n), \quad (3)$$

respectively. The $U_\mu(n)$ represents the link-variable from a site $n = (n_x, n_y, n_z, n_\tau)$ to its neighbor in the μ -direction, and takes the value with the $SU(N_c)$ group elements.

Now, we introduce the twisted boundary conditions in the x and y directions;

$$U_\mu(n + \hat{\nu}L) = \Omega_\nu U_\mu(n) \Omega_\nu^\dagger \text{ for } \nu = x, y, \quad (4)$$

while the ordinary periodic boundary conditions are imposed in the z and τ directions;

$$U_\mu(n + \hat{\nu}L) = U_\mu(n) \text{ for } \nu = z, \tau. \quad (5)$$

Here, L denotes the lattice extent for each direction in lattice unit. For simplicity, only in this subsection, we consider the lattice extents for all directions have the same length. The $SU(N_c)$ matrices, Ω_ν ($\nu = x, y$), are the twist matrices, which have the following properties in the case of $N_c = 3$,

$$\Omega_\nu \Omega_\nu^\dagger = \mathbb{I}, (\Omega_\nu)^3 = \mathbb{I}, \text{Tr}[\Omega_\nu] = 0, \quad \text{and} \quad \Omega_\mu \Omega_\nu = e^{i2\pi/3} \Omega_\nu \Omega_\mu, \quad (6)$$

for a given μ and $\nu (\neq \mu)$.

At the corner on the lattice in the x - y plane, a translation of the link variable is given by

$$U_\mu(n + \hat{x}L + \hat{y}L) = \Omega_x \Omega_y U_\mu(n) \Omega_y^\dagger \Omega_x^\dagger. \quad (7)$$

The interchanging Ω_x and Ω_y in the equation should lead to the same result. The gauge transformation for the original links;

$$U_\mu(n) \rightarrow \Lambda(n) U_\mu(n) \Lambda^\dagger(n + \hat{\mu}) \quad (8)$$

implies

$$\Lambda(n + \hat{\nu}L) = \Omega_\nu \Lambda(n) \Omega_\nu^\dagger. \quad (9)$$

Then, the Wilson-Plaquette gauge action with the twisted boundary conditions at the boundary, for instance $n_y = L - 1$, is given by

$$\begin{aligned} P_{xy} &= U_x(n_x, L - 1, n_z, n_\tau) U_y(n_x + 1, L - 1, n_z, n_\tau) \Omega_y U_x^\dagger(n_x, 0, n_z, n_\tau) \\ &\quad \times \Omega_y^\dagger U_y^\dagger(n_x, L - 1, n_z, n_\tau). \end{aligned} \quad (10)$$

The toron configurations, which are related to the closed winding around the whole torus, are not transformed into themselves by the twisted conditions [10]. In fact, they do not have a degenerate energy with the standard vacuum, since their boundary plaquette gives a different contribution from the standard one.

Next, we consider the gluon propagator in this lattice setup. The link variable can be parameterized by the gauge fields ($A_\mu(n)$) as

$$U_\mu(n) = e^{ig_0 A_\mu(n)}, \quad \text{with } A_\mu^\dagger(n) = A_\mu(n), \quad \text{Tr}[A_\mu(n)] = 0. \quad (11)$$

The plane-wave expansion of the gauge field is given by

$$A_\mu(n) = \frac{1}{L^4} \sum_k \Gamma_k \tilde{A}_\mu(k) e^{ikn + ik_\mu/2}, \quad (12)$$

where Γ_k is a $N_c \times N_c$ complex matrix. The corresponding twisted condition for the gauge field for $\nu = x, y$ implies

$$\Omega_\nu \Gamma_k \Omega_\nu^\dagger = e^{ik_\nu L} \Gamma_k. \quad (13)$$

The non-zero solution is realized only if the momentum components satisfy

$$k_{x,y} = k_{x,y}^{ph} + k_{x,y}^\perp, \quad k_{z,\tau} = k_{z,\tau}^{ph}, \quad (14)$$

where

$$k_\mu = \frac{2\pi m_\mu^{ph}}{L}, \quad k_\mu^\perp = \frac{2\pi m_\mu^\perp}{N_c L}. \quad (15)$$

Here, $-L/2 \leq m_\mu^{ph} < L/2$ denotes an ordinary physical momentum for $\mu = x, y, z$, and τ , while there is an additional unphysical degree of freedom $m_\mu^\perp = 0, 1, N_c - 1$ for the twisted directions. We can find an one-to-one correspondence between the unphysical momenta and the color degrees of freedom of A_μ [14]. In fact, the number of the combination of (k_x^\perp, k_y^\perp) is $N_c^2 - 1$ due to the traceless condition of the gauge field.

If we take the Feynman gauge, then the gluon propagator in the momentum space is

$$\langle \tilde{A}_\mu(q^{ph}, q^\perp) \tilde{A}_\nu(k^{ph}, k^\perp) \rangle = \frac{1}{2N_c} \delta_{(q+k)^{ph}, 0}^{(4)} \delta_{(q+k)^\perp, 0}^{(2)} (1 - \delta_{k^\perp, 0}^{(2)}) e^{-\pi i(k^\perp, k^\perp)/3} \frac{1}{k^2} \delta_{\mu\nu}, \quad (16)$$

where $k^2 = 4 \sum_\mu \sin^2(k_\mu/2)$ and $(\tilde{k}^\perp, k^\perp) = \tilde{m}_x^\perp m_x^\perp + \tilde{m}_y^\perp m_y^\perp + (\tilde{m}_x^\perp + \tilde{m}_y^\perp)(m_x^\perp + m_y^\perp)$. Because of the factor $(1 - \delta_{k^\perp, 0}^{(2)})$, the zero-modes including the torons are excluded in the propagator. Therefore, the IR cutoff proportional to $1/(N_c L)$ in momentum space is induced in this lattice setup.

The IR momentum cutoff is also related with the existence of the fractional instanton on $\mathbb{T}^3 \times S^1$ ($\mathbb{T}^3 \times \mathbb{R}$). According to Ref. [31], all size-moduli of the integer-instanton on \mathbb{R}^4 are associated with the translation-moduli of the fractional-instanton on the compactified spaces ($\mathbb{T}^3 \times \mathbb{R}$). Then, the

fractional-instanton with the smallest instanton number ($Q = 1/N_c$) has no size modulus, and hence the size of fractional-instantons is unique. The size is related with the compactification radius (L). The intuitive understanding of the absence of the size-modulus is the following¹: If the instanton-size is smaller than the compactification radius, then the instanton becomes the ordinary integer-instanton, since the situation is the same with \mathbb{R}^4 spacetime. On the other hand, the large instanton-size is also forbidden, since the gluon has a non-zero “mass” coming from the shifted momentum ($k^\perp \propto 1/L$) of the twisted directions. Then, the size of the fractional instanton with the smallest charge is fixed. The fractional-instanton with the larger charge can be constructed as the composite states of the smallest ones.

In the end of this section, let us show the explicit form of the twist matrices in our numerical calculations [15, 32],

$$\Omega_x = \begin{pmatrix} 0 & 1 & 0 \\ 0 & 0 & 1 \\ 1 & 0 & 0 \end{pmatrix}, \Omega_y = \begin{pmatrix} e^{-i2\pi/3} & 0 & 0 \\ 0 & e^{i2\pi/3} & 0 \\ 0 & 0 & 1 \end{pmatrix}. \quad (17)$$

3 Simulation strategy

3.1 Lattice parameters

The simulation strategy to investigate the nonperturbative properties in the perturbative regime is as follows. We utilize the Wilson-Plaquette gauge action given by Eq. (2) as a lattice gauge action. We put the lattice parameter $\beta = 2N_c/g_0^2$. The other lattice parameters, which we can control by hand, are the lattice extents in spacial (N_s) and temporal directions (N_τ). The lattice spacing “ a ” is put unity during the numerical simulation. Once we introduce the physical quantity as a reference scale, for instance the Sommer scale [33] and t_0 scale in the gradient flow method [34], then we obtain one-to-one correspondence between β and “ a ”.

To investigate a nontrivial semi-classical solution, the lattice parameters (β, N_s, N_τ) satisfy the following three conditions:

- (1) the twisted boundary condition on the two compactified dimensions to introduce the IR momentum cutoff and to kill the toron modes
- (2) sufficiently large lattice-extent to generate a multi-number of the topo-

¹We appreciate K. Yonekura for useful discussions.

logical objects

(3) tuned lattice gauge coupling to realize the perturbative regime

For the condition (1), we use the $N_s^3 \times N_\tau$ lattice, where the twisted boundary condition is imposed to the x and y directions in the three spacial directions. For simplicity, the z -direction has the same lattice extent with the x, y -directions, but its boundary condition is periodic.

The size of the fractional-instanton is predicted as the same with the compactification radius (N_s). Then, to generate the multi-fractional-instanton, for the condition (2), at least one-direction (here N_τ) is N_c -times larger than N_s . We choose $(N_s, N_\tau) = (12, 60)$ for this work.

For the condition (3), we take $\beta = 16$. According to Fig. 4 in Ref. [15], the running coupling constant at the scale ($L_s = aN_s$) indicates $g^2(1/L_s) \approx 0.7$. It is well consistent with the result of the 1-loop approximation, which is independent of the renormalization scheme. If we fix the Λ scale where the running coupling constant in the Twisted-Polyakov-Loop scheme diverges as shown in Ref. [15], the lattice setup with $(\beta, N_s) = (16, 12)$ corresponds to $L_s\Lambda \approx 1.5^{-24}$. It satisfies the Dunne-Ünsal condition, $N_c L_s \Lambda \ll 2\pi$, where the theory is in the weakly coupled regime but still there are some nonperturbative features. The lattice spacing is $a \approx 5.0 \times 10^{-6}$ [fm], if we use $\Lambda = 200$ [MeV]. Then, the box size of this lattice is extremely small, but it would be suitable to study the semi-classical behavior of the gauge theory in the weakly coupled regime. In fact, the action density ($S_W/N_s^3 N_\tau$) is roughly 0.048 in $(\beta, N_s, N_\tau) = (16, 12, 60)$, which is close to the classical limit, where the action takes a minimum value.

3.2 Sampling method of the configurations in high β

To collect the gauge-configuration samples in a weak-coupling regime, we have to care about the autocorrelation problem: a new generated-configuration, which is updated using the random-number series and the old configuration, is very similar with the old one in Montecarlo simulation. The autocorrelation length depends on observables, and generally the quantities related to the low-mode physics have a long autocorrelation. In a typical calculation for the Yang-Mills theory (quenched QCD) at the zero-temperature with $a \approx O(10^{-2})$ [fm], the autocorrelation length of the topological charge is a few ten- or hundred-sweeps (see *e.g.* [35]). The length grows in proportion to $O(1/a^5)$ [35, 36, 37], so that our lattice calculations with $a \approx 5.0 \times 10^{-5}$ must suffer from a severe autocorrelation problem.

To avoid this, we prepare the 100 seeds of random-number generation, here we label them as #1 – #100. We independently update $O(10^3)$ sweeps using each random-number series. Here, we call one sweep as a combination of one Pseudo-Heat-Bath (PHB) update and 10 over-relaxation steps. We collect 100 configurations as samples in a fixed N -th sweep, and we name them “conf.#” using its seed of the random-number series. For the comparison, we also generate the other 100 configurations using the same method and the same lattice parameters, while the boundary conditions are periodic for four directions. From here, we denote “TBC lattice” for the lattice with $(x, y, z, \tau) = (\text{twisted}, \text{twisted}, \text{periodic}, \text{periodic})$ boundaries, while “PBC lattice” for the one with the periodic boundaries for all directions.

4 Results

4.1 Topological charge

The lattice operator of the topological charge defined by Eq. (1) can be written by the clover-leaf operator on the lattice (see Eq.(2.18) in Ref. [38]). The measured topological charge of the quantum gauge configuration, which

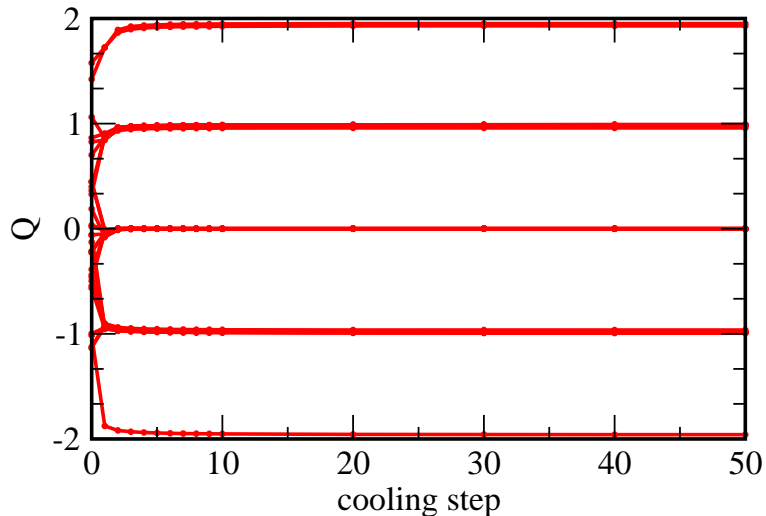


Figure 2: Cooling step dependence of the instanton charge (TBC).

is generated by Montecarlo method, do not take an integer-value, because

of UV fluctuations. We utilize the cooling method [39, 40, 41], that is the evolving step to minimize the gauge action by smoothing the configurations. Figure 2 presents an example plot for the value of Q for several configurations (conf.# 1 – 30) in the TBC lattice as a function of the cooling step. The value of Q rapidly converges to an (almost) integer-value with a few cooling steps. We perform the cooling process until 200 steps and confirm that the plateau continues. Here, the small discrepancy from the exact integer-value, at most $(\Delta Q/Q) \approx 0.04$, comes from the lattice artifacts. In this paper, we neglect the small discrepancy, and identify the value of Q in the plateau of the cooling step as an integer-value.

Now, we fix the number of cooling steps as 50 ($N\text{-cool} = 50$) and the number of sweeps as 2000. The left panel of Fig. 3 shows the result of the PBC lattice. The horizontal axis denotes the configuration-number labeled by the seed of random-series. We see that all configurations have $Q = 0$. On

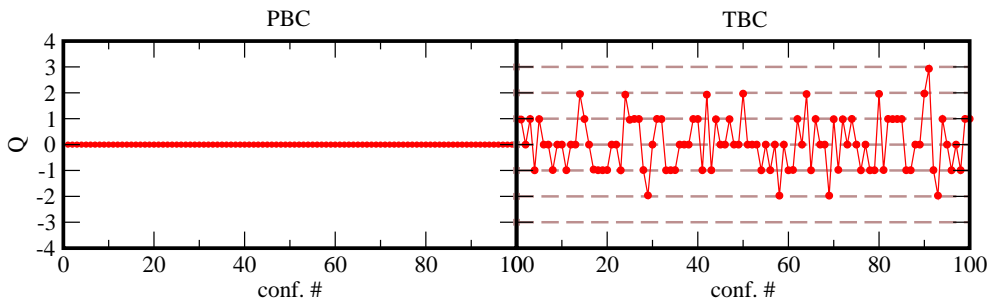


Figure 3: Total instanton charge on the PBC (left) and the TBC (right) lattices for each 100 configuration.

the other hand, there are several configurations with non-zero Q values on the TBC lattice as shown in the right panel of Fig. 3. In our calculation, it distributes $-2 \leq Q \leq 3$. The number of configurations with non-zero topological charges is 66, and the remain 34 configurations live in the $Q = 0$ sector.

Let us focus on the results on the TBC lattice. We found that the charges on each lattice site have a strong τ -dependence in the four-dimensional space-time. Taking the sum only for the three-dimensional spaces, we define a local

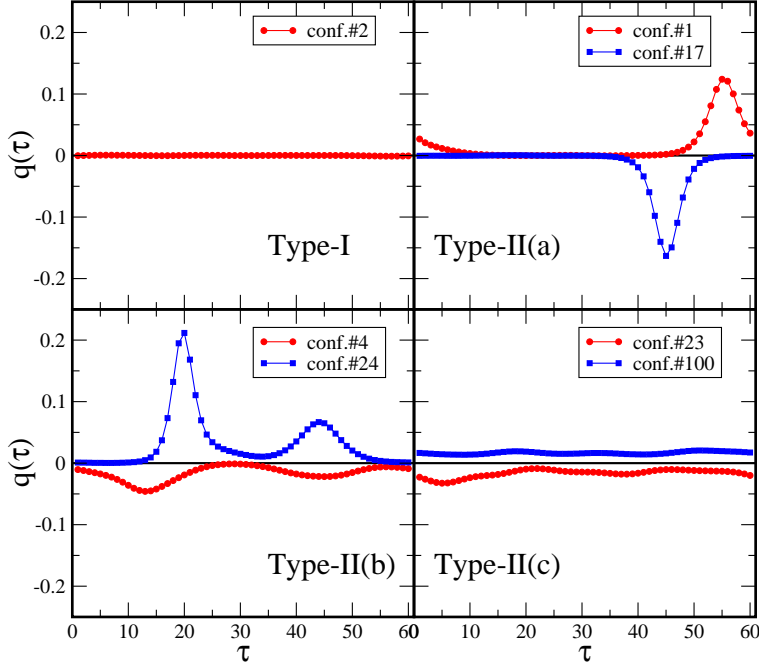


Figure 4: Typical distributions of the local instanton charges. The integer-instanton (and anti-instanton) exists in the right-top panel. On the other hand, one can clearly see that the topological charges is “fractionalized” in the left-bottom panel (see Eq. (19)).

charge,

$$q(\tau) = \frac{1}{32\pi^2} \sum_{x,y,z} \epsilon_{\mu\nu\rho\sigma} F_{\mu\nu}^a F_{\rho\sigma}^a(x, y, z, \tau), \quad (18)$$

as a function of the imaginary-time coordinate. We plot the local charge for several typical configurations in Fig. 4. The left-top panel of Fig. 4 presents the local charge of the configuration with $Q = 0$ (conf.#2). All configurations in the $Q = 0$ sector indicate that its local-charge in every τ -coordinate is also zero. Here, we call them “**Type-I**”. On the other hand, the local charge of the configurations with $Q \neq 0$ can be roughly classified by three types as follows:

Type-II(a): it has a single peak (the right-top panel in Fig. 4)

Type-II(b): it has several peaks (the left-bottom panel)

Type-II(c): it takes a continuous non-zero value (the right-bottom panel)

In the case of **Type-II(a)**, if we take the sum of $q(\tau)$ around the single peak, then the result agrees with (almost) integer and is consistent with the value of Q . For instance, the confs.#1 (red-circle) and #17 (blue-square) have $Q = +1$ and $Q = -1$, respectively. These peaks can be interpreted as the integer instanton and anti-instanton, respectively. In the case of **Type-II(c)**, after summed up to $q(\tau)$ for all τ coordinates, we can find that it gives an integer-value. The sums of $q(\tau)$ in the confs.#23 (red-circle) and #100 (blue-square) shown in Fig. 4 become $Q = -1$ and $Q = +1$, respectively. We find that a uniform behavior for z -direction of the local charge on site-by-site as similar with the one for the action density in Principal Chiral Model given in Ref. [30]. On the other hand, the values of the local charge on all sites display the same order in contrast to the appearance of more than $O(10^2)$ hierarchy in the data of **Type II(a)** and **Type II(b)**.

The configurations in **Type-II(b)** are the most interesting. We can take the sum of $q(\tau)$ for each peak by dividing τ regime into several domains, whose boundaries are the coordinates taking the local minimum of $|q(\tau)|$. Then, each charge takes $n/3$ -value within $\Delta Q/Q \approx 0.04$ error, where n is the integer-value except for a multiple number of 3. The confs.#4 (red-circle) and #24 (blue-square) plotted in Fig. 4 have the total instanton number $Q = -1$ and $Q = +2$, respectively. The local charge for each peak can be calculated by

$$\begin{aligned}
 \text{conf.\#4 : } Q_1 &= \sum_{\tau=29}^{55} q(\tau) = -0.343 \approx -\frac{1}{3}, \\
 Q_2 &= Q - Q_1 = -0.647 \approx -\frac{2}{3}, \\
 \text{conf.\#24 : } Q_1 &= \sum_{\tau=6}^{33} q(\tau) = 1.269 \approx \frac{4}{3}, \\
 Q_2 &= Q - Q_1 = 0.656 \approx \frac{2}{3}.
 \end{aligned} \tag{19}$$

Thus, some instantons with an integer charge contain several fractional-instantons in the weak coupling regime.

To see the fractionality of the charge is not a just quantum fluctuation, let us show the stability of these local fractional-instantons during the cooling processes. Figure 5 displays the local charges (Q_1, Q_2) for the confs.#4 (red-circle) and #24 (blue-square) as a function of cooling step. Although if it is a

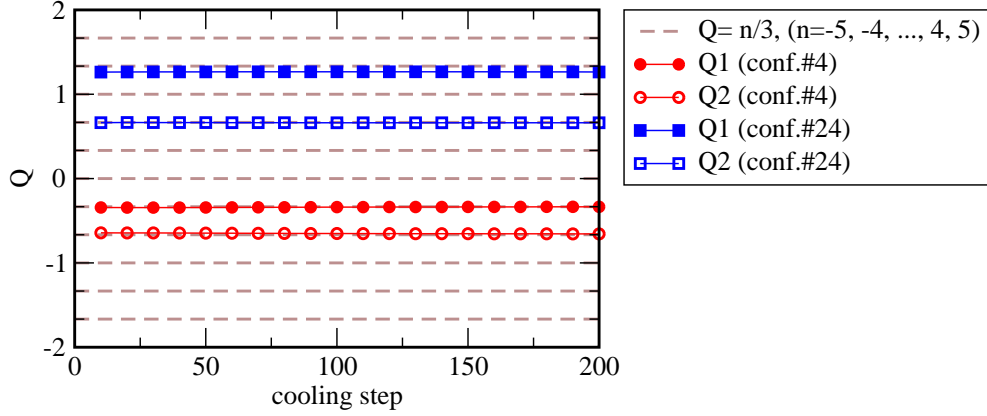


Figure 5: Cooling step dependence of the local charges, Q_1 (filled symbol) and Q_2 (open symbol), for the conf.#4 (red-circle) and #24 (blue-square).

just quantum fluctuation then the charge would disappear by the averaging process, we found that the position of the local minimum of $|q(\tau)|$ and each charge are very stable.

Next, we investigate the topology changing during the PHB updates. In ordinary lattice calculations for the Yang-Mills theory focusing on the strong coupling regime, the total instanton charge can be changed within a few ten or hundred Montecarlo sweeps, since the potential barrier is finite on the lattice. As we explained, the lattice spacing in our calculation is very tiny. The topology changing does not so frequently occurs, but it is happened in $O(10^3)$ sweeps. Furthermore, we found that the local topological charge is rather frequently changed during the PHB updates.

The typical results are shown in Fig. 6. In all panels, the number of cooling processes is fixed as $N\text{-cool}=50$. Let us focus on each color symbol in three panels from the left to the right. The magenta-triangle, blue-square, and red-circle symbols denote the local charge of confs.#1, #91, and #69, respectively. During the PHB updates from 2100-th to 4000-th sweep, the total-charge changes as follows:

$$\begin{aligned}
 \text{conf.\#1} : & \quad Q \text{ does not change } (Q = +1) \\
 \text{conf.\#91} : & \quad Q = +2 \rightarrow Q = +2 \rightarrow Q = +1 \\
 \text{conf.\#69} : & \quad Q = -2 \rightarrow Q = -1 \rightarrow Q = 0
 \end{aligned}$$

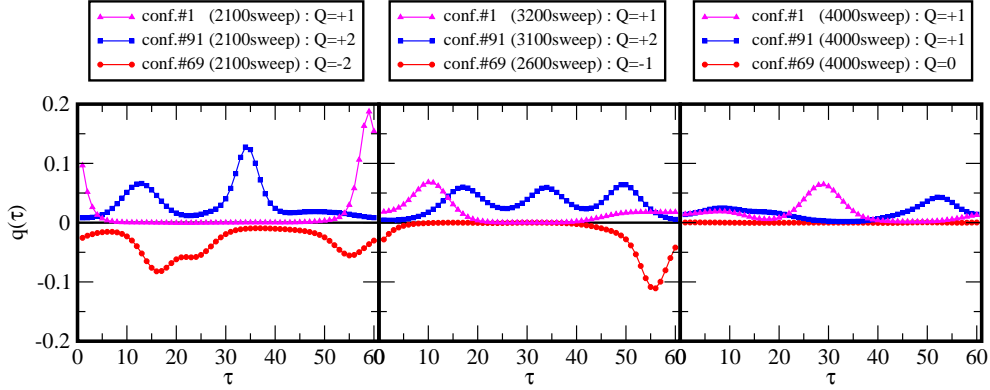


Figure 6: Example plots of the sweep dependence of the local topological charge $q(\tau)$. The magenta-triangle, blue-square, and red-circle symbols denote the configurations, which are generated by the initial random-number #1, #91, and #69, respectively.

Meanwhile, the combination of the local charges indicates a rich variation:

$$\begin{aligned}
 \text{conf.\#1} & \quad (+1 \text{ with single peak}) \rightarrow (+2/3, +1/3) \rightarrow (+2/3, +1/3) \\
 \text{conf.\#91} & \quad (+2/3, +4/3) \rightarrow (+2/3, +2/3, +2/3) \rightarrow (+1/3, +2/3) \\
 \text{conf.\#69} & \quad (-4/3, -2/3) \rightarrow (-1 \text{ with single peak}) \rightarrow (q(\tau) = 0)
 \end{aligned}$$

Thus, the multi-fractional-instanton merges into the integer-instanton and vice versa, and the fractional instanton with a large charge deforms into the multi-fractional one with a small charge.

In fact, in $\mathbb{C}P^{N-1}$ model, it is known that the fractional-instantons can transform into the integer-instanton if the moduli parameter is changed by hand (see Fig. 4 in Ref. [42]). If two fractional-instantons approach to each other and merge into one, then the translation moduli of the fractional-instanton is back to the size-moduli of the integer-instanton. On the other hand, if the size of integer-instanton becomes larger than the radius of the compactified direction, then the integer-instanton divides into two fractional-instantons. We consider that the similar phenomenon dynamically occurs during the Montecarlo simulation for the Yang-Mills theory.

We put three remarks: The first one is related to the bion configuration. We investigated 2100 configurations in total, which are independently generated by using 100 seeds of the random number from 2000-th to 4000-th sweep with the 100-sweep interval. Among them, there is no $Q = 0$ configu-

ration contained by a pair of the fractional-instanton and the fractional-anti-instanton. Such a configuration is called bion, and it plays an important role for the resurgence structure in the $\mathbb{C}P^{N-1}$ model [27, 28]. The absence of the bion will be discussed in the summary section.

The second one is a decrease of the topological charge in the long PHB sweeps. At 2000-th sweep, the number of configurations in the $Q = 0$ and $Q \neq 0$ sectors are 34 and 66, respectively. As increasing the number of sweep, in fact at 4000-th sweeps, the corresponding numbers become 49 and 51. Thus, the number of configurations in the $Q = 0$ sector increases. It might suggest that only the $Q = 0$ sector remains after the infinitely updations. Actually, the self-dual configuration on this lattice setup is not an exact solution, and we need the additional twisted boundary conditions also in the z and τ directions to make it [7]. This situation is the same with the ordinary QCD calculations. If the instanton size is small compared to the extension of the lattice, then we can see the various instanton configurations, since it is not sensitive of the choice of boundary conditions. To see an actual distribution of the topological charges on the two-dimensional twists must be found through the accumulation of the data in the large-volume and the low- β simulations.

The third one is for the size-modulus of the fractional-instanton. According to Ref. [31], there is no size-modulus in the fractional-instantons. Several (exactly 10 in total) fractional-instantons with $Q = \pm 2/3$ are plotted in Figs. 4 and 6. It seems that they all has an unique shape, namely a similar height of the peak and a similar curve around it. The actual data of the peak-height takes between $|q(\tau)| = 0.04$ and $|q(\tau)| = 0.07$. In our analyses, where we neglect at most $\Delta Q/Q \approx 0.04$ error, it is hard to give a solid conclusion beyond the error. On the other hand, some fractional-instantons with the other charges have a broader width. We consider that the lost of the uniqueness of the shape for the fractional-instantons comes from the introduction of an additional one-compact (periodic) direction in comparison with the spacetime structure in Ref. [31]. The periodicity forces the total charge to take an integer-value. This constraint deforms the shape of configuration. We expect that a further large-volume calculation for the temporal direction and the continuum extrapolation will improve the situation, and will reveal the uniqueness of the shape for the fractional-instantons.

4.2 Polyakov loop and center symmetry

The Polyakov loop (P) is the order parameter of the center symmetry breaking, and it changes $P \rightarrow Pe^{2\pi ik/3}$ with $k = 0, 1$, and 2 , under the center transformation. In the PBC lattice, the Polyakov loop in the μ -direction is given by the product of the link variables of the direction;

$$P_\mu = \frac{1}{V} \sum_{\text{sites of } \nu(\neq\mu)} \frac{1}{N_c} \text{Tr} \left[\prod_j U_\mu(\mu = j, \nu) \right]. \quad (20)$$

Here, we take the spacetime average for each configuration, and $V = N_s^3$ for $\mu = \tau$ and $V = N_s^2 \cdot N_\tau$ for the others. On the other hand, because of the twisted boundary condition, the definition of the Polyakov loop in the twisted directions are modified as,

$$P_x = \frac{1}{N_s^2 N_\tau} \sum_{y,z,\tau} \frac{1}{N_c} \text{Tr} \left[\prod_j U_x(x = j, y, z, t) \Omega_x e^{i2\pi y/3L} \right], \quad (21)$$

in order to satisfy the gauge invariance and the translational invariance.

The scatter plots of the Polyakov loop for each direction are given in Fig. 7. Each data point denotes the data for one configuration. Here, all configurations are at 2000-th sweep from the random start. The results for the PBC lattice are shown in the left panels of the figure. The x , y , and z directions are equivalent, so that here we present the Polyakov loop only in the z and τ directions in the left-top and left-bottom panels, respectively. At $\beta = 16$ with $N_s = 12$, it is clearly in the deconfined phase because of its scale ($L_s \Lambda \approx 6.0 \times 10^{-5}$). Then, the Polyakov loop in the z -direction locates in one of three degenerated vacua, whose complex phases are 0 and $\pm 2\pi/3$. In the continuum limit keeping the physical lattice-size, one of them is chosen, therefore the center symmetry is spontaneously broken. This behavior is the same with the situation of the Yang-Mills theory in the high-temperature phase. The Polyakov loop in the τ direction seems to be invariant under the center symmetry, since they locate around the origin.

On the other hand, the right panels in Fig. 7 present the scatter plots of the Polyakov loop in the TBC lattice. The Polyakov loop for the x direction, where the twisted boundary conditions is imposed, is shown in the right-bottom panel. Because of the twist matrix, the Polyakov loop locates around the origin in the complex plane. The result for the y -direction is identical

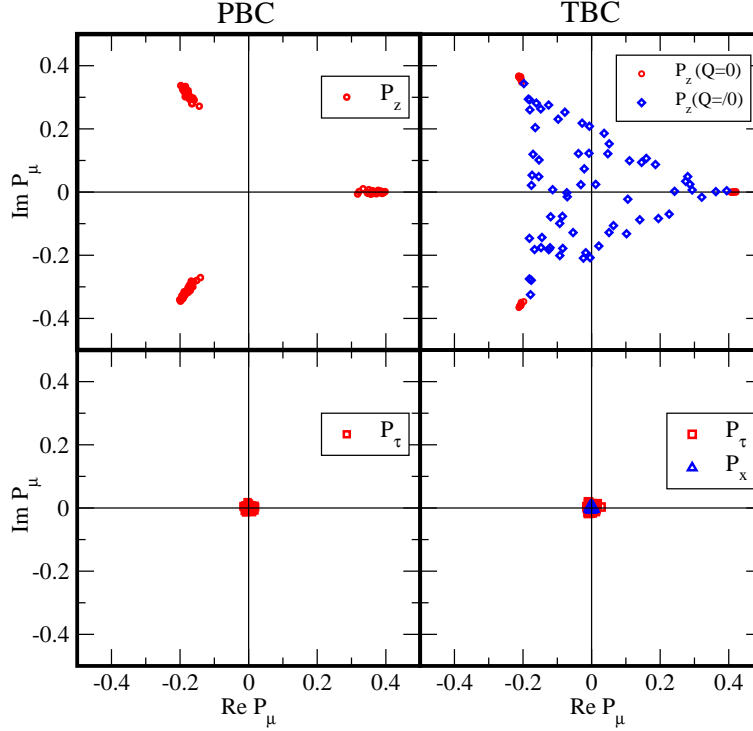


Figure 7: Scatter plot of Polyakov loop for each direction. Left panels denote the spacial (bottom) and the temporal direction (top). All directions have the periodic boundary condition. Right-top panel shows the results for the spacial direction with periodic boundary, while the right-bottom panel gives the ones for the spacial direction with twisted boundary (blue-triangle) and the temporal direction with periodic boundary conditions (red-square).

with the one for the x -direction. For the τ -direction, the behavior is the same with the one in the PBC lattice. The z -direction as shown in the right-top panel indicates a curious behavior, even though the boundary condition for the z -direction is not changed from the PBC lattice. The distribution of the Polyakov loop are spread over the whole (almost) triangle, where the matrix of the Polyakov loop before taking the trace satisfies the unitarity condition. The location of each data is changed under the center symmetric transformation if $|P| \neq 0$, so that the center symmetry of the configurations is generally broken in the same meaning with results of the finite-temperature simulation. However, its breaking structure becomes milder than the one in

the PBC lattice.

Note that in the right-top panel of Fig. 7, the red-circle symbols located in one of the \mathbb{Z}_3 -degenerated vacua denote the configurations with $Q = 0$, while the blue-diamond symbols, which are inside of the triangle, corresponds to the $Q \neq 0$ configurations. The figure clearly suggests that there is a relationship between the value of Q and the Polyakov loop in the z -direction.

4.3 Tunneling behavior and fractional instanton

Now, let us investigate the relationship shown in the end of the previous subsection. We introduce the Polyakov loop in the z -direction on each lattice site;

$$\begin{aligned} \tilde{P}_z(x, y, \tau) &= \frac{1}{N_c} \text{Tr} \left[\prod_j U_z(x, y, z = j, \tau) \right] \\ &\equiv |\tilde{P}_z|(x, y, \tau) e^{i\varphi(x, y, \tau)}. \end{aligned} \quad (22)$$

The histogram of the $\varphi(x, y, \tau)$ for a typical configuration is shown in Fig. 8. Here, the corresponding data of the local charge are displayed in Fig. 4. We see that in the case of **Type-I** and **Type-II(a)**, the site-by-site distribution of the Polyakov loop locates at one of the \mathbb{Z}_3 -degenerated vacua. In the case of **Type-II(a)**, where the integer instanton exists, the tunnel phenomenon is not apparent, since it occurs within a tiny slice of τ -coordinate. The situation is similar with that for an ordinary integer-instanton in the strong coupling regime on \mathbb{T}^4 , where the instanton configuration wind around the whole 2π angle.

On the other hand, in the case of **Type-II(b)** configurations, two of the \mathbb{Z}_3 -degenerated vacua have been chosen. To see the manifest relationship between the fractional-instanton and the distribution of the Polyakov loop, we plot the averaged complex phase of conf.#24 as a function of τ (the blue-circle symbols) in Fig. 9. Here, the averaged complex phase expresses as $\langle \varphi(\tau) \rangle \equiv \sum_{x, y} \varphi(x, y, \tau) / N_s^2$. Simultaneously, we also present the local topological charge $q(\tau)$ as the red-square symbols, where it is multiplied by 20 so as to be easily seen. We can find that if the value of the local charge is almost zero, then $\langle \varphi \rangle$ stays in 0 or $-2\pi/3$ ², while around the peak of

²The small discrepancy of $\langle \varphi(\tau) \rangle$ from $\varphi = -2\pi/3$ at $28 \lesssim \tau \lesssim 40$ comes from the mix with a small excess around $\varphi = +2\pi/3$ in the left-bottom panel of Fig. 8.

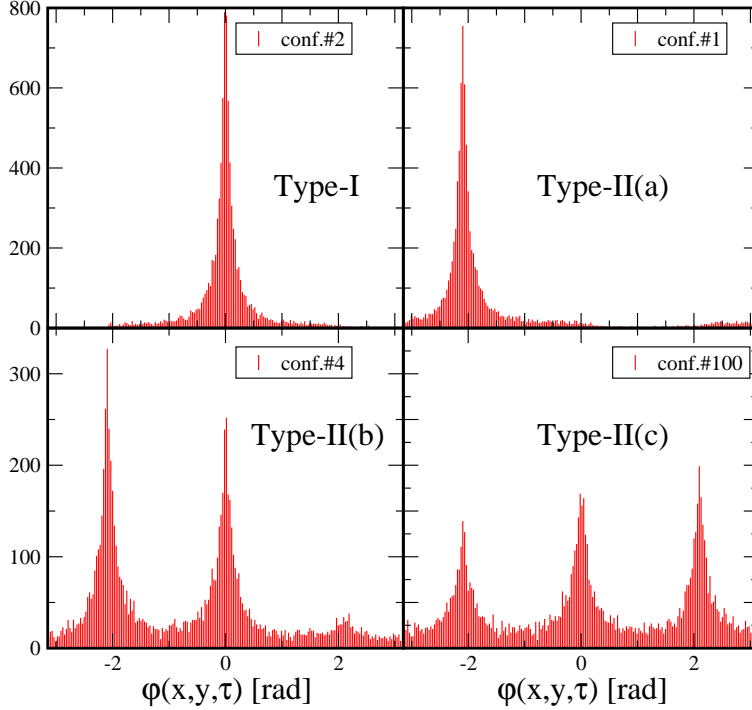


Figure 8: Histogram of $\varphi(x, y, \tau)$ for each type of local charge distributions. The corresponding data of the local charge are shown in Fig 4.

the local charge ($q(\tau)$), where the fractional-instanton exists, the complex phase of the Polyakov loop start changing its value. It describes that the fractional-instanton is related to the tunneling between the \mathbb{Z}_3 -degenerated vacua.

The phenomena occur in the two-dimensional $\mathbb{C}P^{N-1}$ model that can be obtained by the dimensional reduction of the four-dimensional Yang-Mills theory with the twisted boundary conditions [31, 42, 43, 44, 45]. In fact, in the limit where the (x, z) directions shrink, the reduced theory of four-dimensional Yang-Mills becomes the two-dimensional nonlinear sigma model, whose boundary condition in the compactified direction (y) has the \mathbb{Z}_{N_c} -holonomy. The non-zero expectation value of the Polyakov loop for the shrinking direction (z) corresponds to the vacuum expectation value (v.e.v.) of the complex scalar field in the reduced theory, where the v.e.v. depends on the location of τ . The fractional instanton can be interpreted as a classical solution connecting two different $\langle \varphi \rangle$ vacua. Our results in Fig. 9 show that

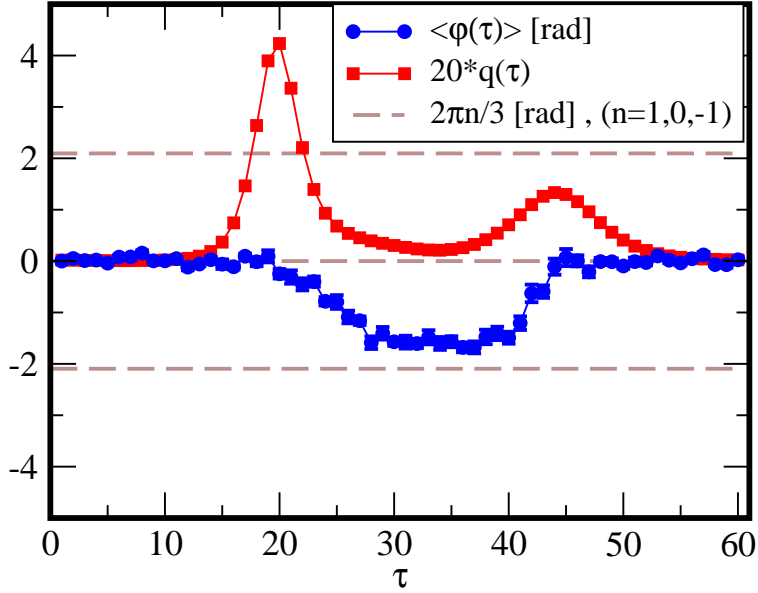


Figure 9: τ -coordinate dependence of the complex phase of the Polyakov loop in z -direction (blue-circle) and the local topological charge (red-square).

the similar interpretation is valid even for the fractional-instantons of the four-dimensional Yang-Mills theory.

In the case of **Type-II(c)**, the histogram of the Polyakov loop on site-by-site has three peaks at three degenerated vacua equally. No clear τ -dependence in the distribution of the Polyakov loop exists, so that we expect that the tunneling behavior among three vacua occurs also through x and y directions. The magnitude of the Polyakov loop given in Eq. (20) is very small ($|P_z| \ll 0.1$), so that the Polyakov loops in all directions locate near the origin in the complex plane. That means the center symmetry in such configurations is dynamically restored. In fact, such a dynamical restoration of the center symmetry is predicted in Ref. [31] on $\mathbb{T}^3 \times \mathbb{R}$ spacetime. In our numerical calculation on $\mathbb{T}^3 \times S^1$ lattice, the appearance rate of **Type-II(c)** configuration is rare, in fact three per one-hundred. Although we naively expect that **Type-II(c)** might be dominant in the continuum and the $S^1 \rightarrow \mathbb{R}$ limits, it must be an important future-work to find which type of configurations remains in the double limits.

4.4 Polyakov loop and confinement

In this section, we focus on the other nonperturbative phenomenon; the confinement. Although the center symmetric distribution described as $|P_\tau| \sim 0$ can be interpreted as a confinement property in the ordinary lattice calculations, we have tuned the value of the lattice parameters to realize the weak coupling regime, where the colored particles can be described by asymptotically free particles. Here, we make a definition of the confinement and the deconfinement in the theory clear, whose center symmetry is restored even in the perturbative regime.

We have seen that the center symmetry seem to be restored by observing the Polyakov loops in the x, y , and τ directions. The center symmetric property in the x and y directions is forced by hand, since it comes from the twist matrices in Eqs. (21). On the other hand, the Polyakov loop in the τ -direction, where a periodic boundary condition is imposed, also indicates the center symmetric property. In our calculation, both z and τ directions have the same periodic boundary condition. Thus, if we take $N_z = N_\tau = 60$ (or $60 \leq N_z \ll N_\tau$), then we could find the Polyakov loops in all directions exhibit the center symmetric distribution.

Generally, the Polyakov loop is related to the free-energy of a single (probe) quark, $P_\tau \propto e^{-N_\tau F_q}$. The large F_q appears in the confined phase, and it diverges in the infinite-volume limit. In our calculation, we take a large lattice extent ($N_\tau = 60$) with an extremely small lattice spacing, so that we have to make the origin of the smallness of $|P_\tau|$ clear; whether it comes from the sizable F_q or the large N_τ with a finite value of F_q .

Figure 10 shows the absolute value of the Polyakov loop in the τ -direction for two lattice parameters; $(\beta, N_s) = (16, 12)$ on the TBC lattice and $(\beta, N_s) = (5, 12)$ on the PBC lattice. It is known that the latter lattice exhibits the confinement behavior, since the critical temperature in the finite temperature simulation is determined as $\beta_c = 6.3384$ in $(N_s, N_\tau) = (\infty, 12)$ [46]. The blue-circle symbols denote the results for the PBC lattices as a function of $1/N_\tau$. We see that all data in $30 \leq N_\tau \leq 80$ are consistent with each other within $2\text{-}\sigma$ statistical error bar, so that there is no N_τ dependence. It is natural in the confined phase, since the Polyakov loop does not feel the lattice extent because of the confinement. On the other hand, the N_τ -dependence of the TBC lattice (red-circle symbols) clearly decreases as increasing N_τ ³.

³We cannot directly compare the absolute values of Polyakov loop between $\beta = 5$ and $\beta = 16$, since the lattice raw data have to be multiplicatively renormalized, where the

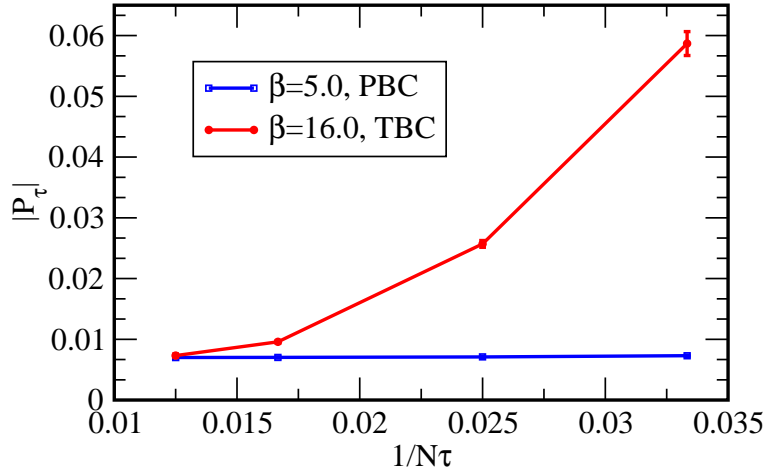


Figure 10: Magnitude of Polyakov loop in τ -direction as a function of N_τ . We take $N_\tau = 30, 40, 60, 80$ from right to left.

The data at $N_\tau = 60$, which we mainly focus on in this work, is still in the middle of its decreasing beyond the statistical error bar. We conclude that the configurations with the fractional-instanton have the deconfinement property as expected.

5 Summary and future works

We have numerically studied the nonperturbative phenomena of the $SU(3)$ gauge theory in the weak coupling regime on $\mathbb{T}^3 \times S^1$ with the large aspect ratio between two radius. Furthermore, we introduce the twisted boundary condition in two directions to realize the perturbative standard vacuum on the hypertorus. The twisted boundary condition induces the IR momentum cutoff for the gluon propagator, and is also related with the existence of the fractional instanton. According to the analogy of the quantum-mechanical models and the low-dimensional quantum field theories, such a deformed spacetime structure might be necessary to see the the resurgence structure. This work is the first step to find a fractional-instanton and its nonperturbative properties within the lattice gauge theory. It looks a promising

renormalization factor depends on the value of β [47].

regularization method to give a well-defined construction of the Yang-Mills theory from the perturbative to the nonperturbative regimes.

The numerical results on the TBC lattice exhibit that the total topological charge (Q) can take nonzero values even in the weak coupling regime, while the PBC lattice calculations with the same lattice parameters generate only the trivial solutions. We have shown that some multi-fractional-instantons locally exist in the configurations with $Q \neq 0$. The fractional-instantons can merge into the integer-instanton and vice versa during the PHB update processes. The fractional-instanton will be a standard integer-instanton in the decompactified limit, since if the lattice extent becomes larger than the confining scale ($\sim 1/\Lambda$), then the situation back to the ordinary zero-temperature calculation in the strong coupling regime.

We have also investigated the center symmetry by observing the Polyakov loop for each spacetime direction. The Polyakov loop in the z -direction on the TBC lattice shows the different behavior from the one on the PBC lattice, though the boundary condition of the direction does not change. The distributions of the Polyakov loop are scattered over the possible unitary triangle in the complex plane. The configuration lives in one of the \mathbb{Z}_3 -degenerated vacua if it has the zero total charge, while the others, whose Polyakov loop locates inside the unitary triangle, correspond to the ones with $Q \neq 0$. We have shown that the local fractional-instanton connects two of the \mathbb{Z}_3 -degenerated phases of the Polyakov loop in the z -direction. On the other hand, the Polyakov loop in the τ -direction seems to be center-symmetric, but its scaling property indicates the deconfinement property. Furthermore, we have found that there are some configurations (**Type-II(c)**), whose Polyakov loops in all directions exhibit the center symmetric property.

For future works, we address following points:

Resurgence structure and renormalon effect

To see a resurgence structure, we would like to find the renormalon pole and its contribution to a physical observable in the perturbative expansion on this twisted spacetime, since it would cancel a contribution of the fractional topological objects in the $Q = 0$ sector. Until now, the perturbative expansion of the plaquette value up to $\mathcal{O}(\alpha^{35})$ has been numerically investigated on \mathbb{T}^4 with the twists in three dimensions using the stochastic perturbation theory [48]. They have determined the normalization of the Borel singularity and estimated the effect of the renormalon to the gluon condensate with a not-so-small error bar. As shown in the present work, the spacetime structure gives a large influence on the physics both qualitatively and quantitatively

in the perturbative regime. Finding the divergent structure and the corresponding effect from the renormalons on $\mathbb{T}^3 \times S^1$ with two-dimensional twists by using a similar calculation with Ref. [48] is a next task .

Adiabatic continuity to the nonperturbative regime

It is expected that the Yang-Mills theory with the twisted boundary condition goes to the ordinary confined phase in the large volume and the strong coupling limit, since in these limits the boundary effects can be negligible. The question is *whether the phase transition occurs between the perturbative and the nonperturbative regimes*. According to the PBC calculation in the context of the finite-temperature Yang-Mills theory, the pure SU(3) gauge theory exhibits the weakly first-order phase transition. However, as shown in §. 4.2 and §. 4.4, the TBC lattice simulation on $\mathbb{T}^3 \times S^1$ indicates a curious behavior: the center symmetry seems to be partially restored even in the weak coupling regime, while the configuration still exhibits the deconfinement property. Furthermore, in comparison with the finite-temperature phase-transition (see Fig. 2 in Ref. [49]), the β -dependence for the Polyakov loop in the TBC lattice with the small lattice size has a gentle downward slope toward the strong coupling regime (shown in Fig. 1 in Ref. [15]). These numerical results on the twisted lattice might suggest the absence of the phase transition toward the decompactified limit, which is conjectured as an adiabatic continuity (Ref. [50] and references therein). In fact, the continuity has been established in the case of $\mathbb{C}P^{N-1}$ and $O(N)$ sigma models in the large- N limit [51].

Other lattice calculations to find a fractional instanton: Schrödinger functional boundary, the four-dimensional twisted, and other approaches

It might be worth to mention the other formulations, which show the fractional instantons on the lattice.

The most popular lattice setup, which connect to the perturbative vacuum, is the one with the Schrödinger functional boundary condition [12]. The similar discussion with this work might be possible by using the lattice setup with the Schrödinger functional boundary with a large aspect ratio between the extents of the spacial and temporal directions. At that time, the zero mode still remains on the lattice with the ordinary Schrödinger-functional boundary condition, then to find the fractional-instanton it may need an additional gauge fixing or the other technique [52] to kill all zero modes and to stabilize the fractional-instanton.

We can also consider the twisted boundary condition for three or four

directions. In fact, although it has been discussed in the strong coupling regime, the lattice numerical simulations with four-dimensional twists have been carried successfully for the $SU(N_c)$ pure gauge theories. The fractional instanton and the action density have been observed [53, 54]. Note that the theory with four-dimensional twisted boundary conditions locally has the same gauge symmetry with $SU(N_c)$, but the global symmetry becomes $SU(N_c)/\mathbb{Z}_{N_c}$. On the other hand, the three-dimensional twisted lattice still keep the same global symmetry with the $SU(N_c)$. As same as our calculation, the total Q on the lattice with three-dimensional twists always takes an interval. On the other hand, the discussions in §. 4.2 and §. 4.3 of this work will be changed, since the additional twisted boundary condition for the z -direction must deform the distribution of Polyakov loop in the z -direction.

The other approaches to find the fractional topological charge on the lattice have been done by using the Dirac operator with the higher-dimensional representations on the periodic lattices [55, 56, 57]. The index theorem for the higher-dimensional Dirac operator and the one for fundamental representation are related with each other, where the color degree of freedom appears as a factor between them. Furthermore, the caloron solution at the finite temperature with a nontrivial homonomy has also been constructed [58, 59, 60, 61]. The energy density and the zero-mode density of the caloron for the $SU(2)$ and $SU(3)$ gauge theories have been numerically investigated [62].

Finding bion configurations

We cannot find a pair of instanton and anti-instanton with neither integer nor fractional charge in the $Q = 0$ sector, so that there is no evidence of the bion configuration in our simulation. In the resurgence scenario, the existence of the bion is important since the fluctuation around such configurations is one candidate of the renormalon. In the case of the integer instanton and anti-instanton, the force between them is attractive, so that it easily annihilates each other if the distance of them is short. We expect that the force between the fractional ones is also attractive, and then the similar phenomena might occur in our simulation. We consider that the bion will appear in the decompactified limit of the temporal direction.

On the other hand, the reduced theory of the four-dimensional Yang-Mills theory, namely two-dimensional CP^{N-1} model with the twisted boundary condition, suggests the sign of the potential depends on the relative phase between the fractional-instanton and fractional-anti-instanton [24, 26, 27]. The large volume simulation and the study on the dynamics between the fractional-instantons for the Yang-Mills theory are interesting future works.

Including the dynamical quarks: \mathbb{Z}_{N_c} -QCD and adjoint QCD

One of the most important directions is to find a similar fractional topological object in the QCD(-like) theories; namely including the dynamical fermions. It is known that there are at least two promising models; the \mathbb{Z}_{N_c} -QCD [63, 64] and the adjoint QCD models [50, 65, 66, 67]. Both theories have the exact center symmetry of the $SU(N_c)$ gauge group in the action, so that we expect that the similar \mathbb{Z}_{N_c} -degenerated vacua and the corresponding fractional instanton might appear in the weak coupling regime.

The formulation of the two-dimensional twists can extend to the system including the dynamical fermions [68]. Actually, in the case of the fundamental fermions, the numerical simulation for the $SU(3)$ gauge theory coupled to $N_f = 12$ with the staggered (Kogut-Susskind) fermions has been carried out [15]⁴. If we utilize the other lattice fermions, it is possible to reduce the number of the fermions using the exact algorithm. The advantage of the usage of the twisted boundary conditions is not only for the absence of toron but also for the induced IR momentum cutoff, as we explained. Then, we can perform the simulation with the exact massless fermions. It must be helpful to investigate the adiabatic continuity near the massless limit as discussed in Ref. [50].

Acknowledgment

The author appreciates S. Aoki and K. Yonekura for deeply discussions about the lattice numerical data, and would like to thank T. Fujimori, T. Misumi, M. Nitta, N. Sakai, and M. Yamazaki for valuable comments. We are also indebted to S. Aoki, T. Misumi, K. Nagata and N. Sakai for helpful comments on this manuscript. The author is grateful to the organizers and participants of RIMS-iTHEMS International Work-shop on Resurgence Theory at RIKEN, Kobe for giving her a chance to deepen their ideas. In particular, the talk given by K. Yonekura at the workshop and the private conversation were invaluable to start this work. Numerical simulations were performed on SX-ACE at the Research Center for Nuclear Physics (RCNP), Osaka University. This work is supported by the Ministry of Education, Culture, Sports, Science, and Technology (MEXT)-Supported Program for the Strategic Research Foundation at Private Universities Topological Science (Grant No.

⁴Note that the $N_f = 12$ theory has an IR fixed point, and it is not QCD(-like) theory.

S1511006), and is also supported in part by the Japan Society for the Promotion of Science (JSPS) Grant-in-Aid for Scientific Research (KAKENHI) Grant Number 18H01217.

References

- [1] M. F. Atiyah and I. M. Singer, “The Index of Elliptic Operators. 1,” *Annals Math.* **87** (1968) 484. doi:10.2307/1970715
- [2] M. Luscher, “Topology of Lattice Gauge Fields,” *Commun. Math. Phys.* **85** (1982) 39. doi:10.1007/BF02029132
- [3] B. Alles, M. D’Elia and A. Di Giacomo, “Topological Susceptibility at Zero and Finite T in $SU(3)$ Yang-Mills Theory,” *Nucl. Phys. B* **494** (1997) 281 Erratum: [*Nucl. Phys. B* **679** (2004) 397] doi:10.1016/S0550-3213(97)00205-8, 10.1016/j.nuclphysb.2003.11.018 [hep-lat/9605013].
- [4] S. Durr, Z. Fodor, C. Hoelbling and T. Kurth, “Precision Study of the $SU(3)$ Topological Susceptibility in the Continuum,” *JHEP* **0704** (2007) 055 doi:10.1088/1126-6708/2007/04/055 [hep-lat/0612021].
- [5] M. Fukugita, M. Okawa and A. Ukawa, “Order of the Deconfining Phase Transition in $SU(3)$ Lattice Gauge Theory,” *Phys. Rev. Lett.* **63** (1989) 1768. doi:10.1103/PhysRevLett.63.1768
- [6] M. Fukugita, M. Okawa and A. Ukawa, “Finite Size Scaling Study of the Deconfining Phase Transition in Pure $SU(3)$ Lattice Gauge Theory,” *Nucl. Phys. B* **337** (1990) 181. doi:10.1016/0550-3213(90)90256-D
- [7] G. ’t Hooft, “Some Twisted Selfdual Solutions for the Yang-Mills Equations on a Hypertorus,” *Commun. Math. Phys.* **81** (1981) 267. doi:10.1007/BF01208900
- [8] G. ’t Hooft, “A Property of Electric and Magnetic Flux in Nonabelian Gauge Theories,” *Nucl. Phys. B* **153** (1979) 141. doi:10.1016/0550-3213(79)90595-9
- [9] M. Luscher and P. Weisz, “Efficient Numerical Techniques for Perturbative Lattice Gauge Theory Computations,” *Nucl. Phys. B* **266** (1986) 309. doi:10.1016/0550-3213(86)90094-5

- [10] A. Gonzalez-Arroyo, J. Jurkiewicz and C. P. Korthals-Altes, “Ground State Metamorphosis For Yang-mills Fields On A Finite Periodic Lattice,” Proc. of the Freiburg NATO Summer Institute 1981
- [11] A. Coste, A. Gonzalez-Arroyo, J. Jurkiewicz and C. P. Korthals Altes, “Zero Momentum Contribution to Wilson Loops in Periodic Boxes,” Nucl. Phys. B **262** (1985) 67. doi:10.1016/0550-3213(85)90064-1
- [12] M. Luscher, R. Narayanan, P. Weisz and U. Wolff, “The Schrödinger Functional: a Renormalizable Probe for Nonabelian Gauge Theories,” Nucl. Phys. B **384** (1992) 168 doi:10.1016/0550-3213(92)90466-O [hep-lat/9207009].
- [13] M. Luscher, R. Sommer, P. Weisz and U. Wolff, “A Precise Determination of the Running Coupling in the $SU(3)$ Yang-Mills Theory,” Nucl. Phys. B **413** (1994) 481 doi:10.1016/0550-3213(94)90629-7 [hep-lat/9309005].
- [14] G. M. de Divitiis, R. Frezzotti, M. Guagnelli and R. Petronzio, “A Definition of the Running Coupling Constant in a Twisted $SU(2)$ Lattice Gauge Theory,” Nucl. Phys. B **422** (1994) 382 doi:10.1016/0550-3213(94)00126-X [hep-lat/9312085].
- [15] E. Itou, “Properties of the Twisted Polyakov Loop Coupling and the Infrared Fixed Point in the $SU(3)$ Gauge Theories,” PTEP **2013** (2013) no.8, 083B01 doi:10.1093/ptep/ptt053 [arXiv:1212.1353 [hep-lat]].
- [16] E. B. Bogomolny, “Calculation Of Instanton - Anti-instanton Contributions In Quantum Mechanics,” Phys. Lett. B **91**, 431 (1980).
- [17] J. Zinn-Justin, “Multi - Instanton Contributions in Quantum Mechanics,” Nucl. Phys. B **192**, 125 (1981).
- [18] G. 't Hooft, “Can We Make Sense Out of Quantum Chromodynamics?,” Subnucl. Ser. **15**, 943 (1979).
- [19] M. Beneke, “Renormalons,” Phys. Rept. **317**, 1 (1999) [hep-ph/9807443].

- [20] P. C. Argyres and M. Unsal, “The Semi-Classical Expansion and Resurgence in Gauge Theories: New Perturbative, Instanton, Bion, and Renormalon Effects,” JHEP **1208** (2012) 063 doi:10.1007/JHEP08(2012)063 [arXiv:1206.1890 [hep-th]].
- [21] G. V. Dunne and M. Ünsal, “Resurgence and Trans-Series in Quantum Field Theory: the $\mathbb{C}P(N-1)$ Model,” JHEP **1211** (2012) 170 doi:10.1007/JHEP11(2012)170 [arXiv:1210.2423 [hep-th]].
- [22] G. V. Dunne and M. Ünsal, “Continuity and Resurgence: Towards a Continuum Definition of the $\mathbb{C}P(N-1)$ Model,” Phys. Rev. D **87** (2013) 025015 doi:10.1103/PhysRevD.87.025015 [arXiv:1210.3646 [hep-th]].
- [23] G. V. Dunne and M. Ünsal, “Generating Non-perturbative Physics from Perturbation Theory,” Phys. Rev. D **89**, 041701 (2014) [arXiv:1306.4405 [hep-th]].
- [24] T. Misumi, M. Nitta and N. Sakai, “Resurgence in sine-Gordon quantum mechanics: Exact agreement between multi-instantons and uniform WKB,” JHEP **1509**, 157 (2015) [arXiv:1507.00408 [hep-th]].
- [25] G. V. Dunne and M. Unsal, “Deconstructing zero: resurgence, supersymmetry and complex saddles,” JHEP **1612** (2016) 002 [arXiv:1609.05770 [hep-th]].
- [26] T. Misumi, M. Nitta and N. Sakai, “Neutral Bions in the $\mathbb{C}P^{N-1}$ Model,” JHEP **1406** (2014) 164 doi:10.1007/JHEP06(2014)164 [arXiv:1404.7225 [hep-th]].
- [27] T. Fujimori, S. Kamata, T. Misumi, M. Nitta and N. Sakai, “Nonperturbative contributions from complexified solutions in $\mathbb{C}P^{N-1}$ models,” Phys. Rev. D **94**, no. 10, 105002 (2016) [arXiv:1607.04205 [hep-th]].
- [28] T. Fujimori, S. Kamata, T. Misumi, M. Nitta and N. Sakai, “Exact Resurgent Trans-series and Multi-Bion Contributions to All Orders,” Phys. Rev. D **95**, no. 10, 105001 (2017) arXiv:1702.00589 [hep-th].
- [29] T. Fujimori, S. Kamata, T. Misumi, M. Nitta and N. Sakai, “Resurgence Structure to All Orders of Multi-Bions in Deformed SUSY Quantum Mechanics,” PTEP **2017** (2017) no.8, 083B02 doi:10.1093/ptep/ptx101 [arXiv:1705.10483 [hep-th]].

- [30] P. V. Buividovich and S. N. Valgushev, “Lattice Study of Continuity and Finite-Temperature Transition in Two-Dimensional $SU(N) \times SU(N)$ Principal Chiral Model,” arXiv:1706.08954 [hep-lat].
- [31] M. Yamazaki and K. Yonekura, “From 4D Yang-Mills to 2D $\mathbb{C}\mathbb{P}^{N-1}$ Model: IR Problem and Confinement at Weak Coupling,” JHEP **1707** (2017) 088 doi:10.1007/JHEP07(2017)088 [arXiv:1704.05852 [hep-th]].
- [32] H. D. Trottier, N. H. Shakespeare, G. P. Lepage and P. B. Mackenzie, “Perturbative Expansions from Monte Carlo Simulations at Weak Coupling: Wilson Loops and the Static Quark Selfenergy,” Phys. Rev. D **65** (2002) 094502 doi:10.1103/PhysRevD.65.094502 [hep-lat/0111028].
- [33] R. Sommer, “A New Way to Set the Energy Scale in Lattice Gauge Theories and Its Applications to the Static Force and Alpha-S in $SU(2)$ Yang-Mills Theory,” Nucl. Phys. B **411** (1994) 839 doi:10.1016/0550-3213(94)90473-1 [hep-lat/9310022].
- [34] M. Lüscher, “Properties and Uses of the Wilson Flow in Lattice QCD,” JHEP **1008** (2010) 071 Erratum: [JHEP **1403** (2014) 092] doi:10.1007/JHEP08(2010)071, 10.1007/JHEP03(2014)092 [arXiv:1006.4518 [hep-lat]].
- [35] S. Schaefer *et al.* [ALPHA Collaboration], “Critical Slowing Down and Error Analysis in Lattice QCD Simulations,” Nucl. Phys. B **845** (2011) 93 doi:10.1016/j.nuclphysb.2010.11.020 [arXiv:1009.5228 [hep-lat]].
- [36] L. Del Debbio, H. Panagopoulos and E. Vicari, “Theta Dependence of $SU(N)$ Gauge Theories,” JHEP **0208** (2002) 044 doi:10.1088/1126-6708/2002/08/044 [hep-th/0204125].
- [37] M. Luscher, “Topology, the Wilson Flow and the Hmc Algorithm,” PoS LATTICE **2010** (2010) 015 doi:10.22323/1.105.0015 [arXiv:1009.5877 [hep-lat]].
- [38] M. Luscher, S. Sint, R. Sommer and P. Weisz, “Chiral Symmetry and $O(A)$ Improvement in Lattice QCD,” Nucl. Phys. B **478** (1996) 365 doi:10.1016/0550-3213(96)00378-1 [hep-lat/9605038].

- [39] B. Berg, “Dislocations and Topological Background in the Lattice $O(3)$ σ Model,” Phys. Lett. **104B** (1981) 475. doi:10.1016/0370-2693(81)90518-9
- [40] Y. Iwasaki and T. Yoshie, “Instantons and Topological Charge in Lattice Gauge Theory,” Phys. Lett. **131B** (1983) 159. doi:10.1016/0370-2693(83)91111-5
- [41] M. Teper, “Instantons in the Quantized $SU(2)$ Vacuum: a Lattice Monte Carlo Investigation,” Phys. Lett. **162B** (1985) 357. doi:10.1016/0370-2693(85)90939-6
- [42] M. Eto, T. Fujimori, Y. Isozumi, M. Nitta, K. Ohashi, K. Ohta and N. Sakai, “Non-Abelian Vortices on Cylinder: Duality Between Vortices and Walls,” Phys. Rev. D **73** (2006) 085008 doi:10.1103/PhysRevD.73.085008 [hep-th/0601181].
- [43] M. Eto, Y. Isozumi, M. Nitta, K. Ohashi and N. Sakai, “Instantons in the Higgs Phase,” Phys. Rev. D **72** (2005) 025011 doi:10.1103/PhysRevD.72.025011 [hep-th/0412048].
- [44] F. Bruckmann, “Instanton Constituents in the $O(3)$ Model at Finite Temperature,” Phys. Rev. Lett. **100** (2008) 051602 doi:10.1103/PhysRevLett.100.051602 [arXiv:0707.0775 [hep-th]].
- [45] W. Brendel, F. Bruckmann, L. Janssen, A. Wipf and C. Wozar, “Instanton Constituents and Fermionic Zero Modes in Twisted Cp^N Models,” Phys. Lett. B **676** (2009) 116 doi:10.1016/j.physletb.2009.04.055 [arXiv:0902.2328 [hep-th]].
- [46] G. Boyd, J. Engels, F. Karsch, E. Laermann, C. Legeland, M. Lutgemeier and B. Petersson, “Thermodynamics of $SU(3)$ Lattice Gauge Theory,” Nucl. Phys. B **469** (1996) 419 doi:10.1016/0550-3213(96)00170-8 [hep-lat/9602007].
- [47] S. Gupta, K. Huebner and O. Kaczmarek, “Renormalized Polyakov Loops in Many Representations,” Phys. Rev. D **77** (2008) 034503 doi:10.1103/PhysRevD.77.034503 [arXiv:0711.2251 [hep-lat]].
- [48] G. S. Bali, C. Bauer and A. Pineda, “Perturbative Expansion of the Plaquette to $\mathcal{O}(\alpha^{35})$ in Four-Dimensional $SU(3)$ Gauge Theory,” Phys. Rev.

- D **89** (2014) 054505 doi:10.1103/PhysRevD.89.054505 [arXiv:1401.7999 [hep-ph]].
- [49] J. B. Kogut, M. Stone, H. W. Wyld, W. R. Gibbs, J. Shigemitsu, S. H. Shenker and D. K. Sinclair, “Deconfinement and Chiral Symmetry Restoration at Finite Temperatures in $SU(2)$ and $SU(3)$ Gauge Theories,” Phys. Rev. Lett. **50** (1983) 393. doi:10.1103/PhysRevLett.50.393
- [50] G. Bergner, S. Piemonte and M. Ünsal, “Adiabatic Continuity and Confinement in Supersymmetric Yang-Mills Theory on the Lattice,” arXiv:1806.10894 [hep-lat].
- [51] T. Sulejmanpasic, “Global Symmetries, Volume Independence, and Continuity in Quantum Field Theories,” Phys. Rev. Lett. **118** (2017) no.1, 011601 doi:10.1103/PhysRevLett.118.011601 [arXiv:1610.04009 [hep-th]].
- [52] S. Aoki, R. Frezzotti and P. Weisz, “Computation of the Improvement Coefficient $C(Sw)$ to One Loop with Improved Gluon Actions,” Nucl. Phys. B **540** (1999) 501 doi:10.1016/S0550-3213(98)00742-1 [hep-lat/9808007].
- [53] M. Garcia Perez, A. Gonzalez-Arroyo and B. Soderberg, “Minimum Action Solutions for $SU(2)$ Gauge Theory on the Torus with Nonorthogonal Twist,” Phys. Lett. B **235** (1990) 117. doi:10.1016/0370-2693(90)90106-G
- [54] P. de Forcrand and O. Jahn, “Comparison of $SO(3)$ and $SU(2)$ Lattice Gauge Theory,” Nucl. Phys. B **651** (2003) 125 doi:10.1016/S0550-3213(02)01123-9 [hep-lat/0211004].
- [55] R. G. Edwards, U. M. Heller and R. Narayanan, “Evidence for Fractional Topological Charge in $SU(2)$ Pure Yang-Mills Theory,” Phys. Lett. B **438** (1998) 96 doi:10.1016/S0370-2693(98)00951-4 [hep-lat/9806011].
- [56] Z. Fodor, K. Holland, J. Kuti, D. Negradi and C. Schroeder, “Topology and Higher Dimensional Representations,” JHEP **0908** (2009) 084 doi:10.1088/1126-6708/2009/08/084 [arXiv:0905.3586 [hep-lat]].

- [57] R. Kitano, T. Suyama and N. Yamada, “ $\theta = \pi$ in $SU(N)/\mathbb{Z}_N$ Gauge Theories,” JHEP **1709** (2017) 137 doi:10.1007/JHEP09(2017)137 [arXiv:1709.04225 [hep-th]].
- [58] K. M. Lee, “Instantons and Magnetic Monopoles on $R^3 \times S^1$ with Arbitrary Simple Gauge Groups,” Phys. Lett. B **426** (1998) 323 doi:10.1016/S0370-2693(98)00283-4 [hep-th/9802012].
- [59] K. M. Lee and C. H. Lü, “ $SU(2)$ Calorons and Magnetic Monopoles,” Phys. Rev. D **58** (1998) 025011 doi:10.1103/PhysRevD.58.025011 [hep-th/9802108].
- [60] T. C. Kraan and P. van Baal, “Exact T Duality Between Calorons and Taub - Nut Spaces,” Phys. Lett. B **428** (1998) 268 doi:10.1016/S0370-2693(98)00411-0 [hep-th/9802049].
- [61] T. C. Kraan and P. van Baal, “Periodic Instantons with Nontrivial Holonomy,” Nucl. Phys. B **533** (1998) 627 doi:10.1016/S0550-3213(98)00590-2 [hep-th/9805168].
- [62] F. Bruckmann, D. Negradi and P. van Baal, “Instantons and Constituent Monopoles,” Acta Phys. Polon. B **34** (2003) 5717 [hep-th/0309008].
- [63] H. Kouno, K. Kashiwa, J. Takahashi, T. Misumi and M. Yahiro, “Understanding QCD at High Density from a Z_3 -Symmetric QCD-Like Theory,” Phys. Rev. D **93** (2016) no.5, 056009 doi:10.1103/PhysRevD.93.056009 [arXiv:1504.07585 [hep-ph]].
- [64] T. Iritani, E. Itou and T. Misumi, “Lattice Study on QCD-Like Theory with Exact Center Symmetry,” JHEP **1511** (2015) 159 doi:10.1007/JHEP11(2015)159 [arXiv:1508.07132 [hep-lat]].
- [65] G. Cossu and M. D’Elia, “Finite Size Phase Transitions in QCD with Adjoint Fermions,” JHEP **0907** (2009) 048 doi:10.1088/1126-6708/2009/07/048 [arXiv:0904.1353 [hep-lat]].
- [66] G. Cossu, H. Hatanaka, Y. Hosotani and J. I. Noaki, “Polyakov Loops and the Hosotani Mechanism on the Lattice,” Phys. Rev. D **89** (2014) no.9, 094509 doi:10.1103/PhysRevD.89.094509 [arXiv:1309.4198 [hep-lat]].

- [67] G. Cossu, E. Itou, H. Hatanaka, Y. Hosotani and J. I. Noaki, “Hosotani Mechanism on the Lattice,” PoS LATTICE **2013** (2014) 103 doi:10.22323/1.187.0103 [arXiv:1311.0079 [hep-lat]].
- [68] G. Parisi, Published in Cargese Summer Inst. 1983:0531, “Prolegomena To Any Future Computer Evaluation Of The QCD Mass Spectrum,”